

Department of Physics and Astronomy
Heidelberg University

Bachelor thesis in Physics
submitted by

Benjamin Bentner

born in Germersheim

**Study of the performance of a kinematic
constraint reconstruction of the missing
momentum in partially reconstructed events in
 $\Lambda_b^0 \rightarrow \Lambda_c^+ \bar{D}^{0*} K^-$ decays**

This bachelor thesis has been carried out by

Benjamin Bentner

at the

Physikalisches Institut Heidelberg

at

Heidelberg University

under the supervision of

Dr. Sebastian Neubert

Study of the performance of a kinematic constraint reconstruction of the missing momentum in partially reconstructed events in $\Lambda_b^0 \rightarrow \Lambda_c^+ \bar{D}^{0*} K^-$ decays

Benjamin Bentner

Abstract

The focus of this bachelor thesis is the presentation and examination of an analysis strategy for a pentaquark search in $\Lambda_b^0 \rightarrow \Lambda_c^+ (\bar{D}^{0*} \rightarrow \bar{D}^0 \pi^0/\gamma) K^-$ decays. The $\Lambda_c^+ \bar{D}^{0*}$ channel in this decay is predicted to couple to the pentaquark state P_c^+ . The kinematic effects of a reconstruction method applied to partially reconstructed events under two hypotheses of missing particles were examined and determined. In this context, a model describing the resolution of the Dalitz plot in the variables $m_{\Lambda_c^+ \bar{D}^{0(*)}}^2$ and $m_{\bar{D}^{0(*)} K^-}^2$ was found for multiple scenarios. Lastly, the applicability of the sPlot technique for background subtraction in the given decay was evaluated. It was found that the full reconstruction of the events in this decay does not allow for the sPlot technique to be used, which is why a different method of background subtraction will have to be found.

Zusammenfassung

In dieser Bachelorarbeit wird eine Strategie zur Analyse für eine Suche nach Pentaquark Zuständen im Zerfall $\Lambda_b^0 \rightarrow \Lambda_c^+ (\bar{D}^{0*} \rightarrow \bar{D}^0 \pi^0/\gamma) K^-$ erarbeitet. Es wird erwartet, dass der Pentaquark Zustand P_c^+ im Kanal $\Lambda_c^+ \bar{D}^{0*}$ des Zerfalles auftritt. Die kinematischen Effekte einer Rekonstruktionsmethode für nicht vollständig rekonstruierte Ereignisse unter zwei verschiedenen Hypothesen wurden untersucht und bestimmt. In diesem Zusammenhang wurde ein Model gefunden, das die Auflösung des Dalitzplot in den Variablen $m_{\Lambda_c^+ \bar{D}^{0(*)}}^2$ und $m_{\bar{D}^{0(*)} K^-}^2$ für unterschiedliche Szenarien beschreibt. Zuletzt wurde die Verwendbarkeit der sPlot Methode für die Unterdrückung des Untergrunds im gegebenen Zerfall untersucht. Aufgrund der Art der vollen Rekonstruktion dieser Zerfälle ist es nicht möglich die sPlot Methode zu verwenden, weshalb eine andere Art der Unterdrückung des Untergrunds gefunden werden muss.

Contents

1	Introduction	1
2	Introduction to the Standard Model of particle physics	3
2.1	The particles of the Standard Model	3
2.2	The fundamental forces	4
3	Detector	6
3.1	The LHCb Detector	6
4	Search for exotics	11
4.1	Pentaquark search	11
4.2	Pentaquark models	12
5	The $\Lambda_b^0 \rightarrow \Lambda_c^+ \bar{D}^{0(*)} K^-$ decay	13
5.1	The $\Lambda_b^0 \rightarrow \Lambda_c^+ \bar{D}^0 K^-$ analysis	13
5.2	$\bar{D}^{0*} \rightarrow \bar{D}^0 \pi^0/\gamma$	14
6	Analysis Strategy	15
6.1	Reconstruction of the \bar{D}^{0*}	15
6.2	Dalitz plot	16
6.3	Monte Carlo Data	17
6.4	Generation of a dataset for $\Lambda_b^0 \rightarrow \Lambda_c^+ \bar{D}^{0*} K^-$	17
6.5	Probability density function	20
7	Efficiency of the reconstruction method	22
8	Resolution	24
8.1	Resolution Model	25
8.2	Different cases	26
8.3	Range	28
9	Background	30
9.1	sPlot technique	30
9.2	From sWeights to probabilities	31
9.3	sWeight averaging	31
10	Conclusion and Outlook	34
	Bibliography	I

Introduction

The Standard Model of particle physics summarizes the current knowledge of fundamental particles and the forces that effect them, with the exception of gravity. The electromagnetic and the weak and strong nuclear force are mediated by gauge bosons which are part of the Standard Model as well as fermions which are the fundamental particles that make up matter in the universe. This is explained in more detail in chapter 2.

In nature, quarks, which represent half of the fundamental fermions, can only exist in states that are color neutral. Therefore at least two quarks have to be confined in a colorless physical state. Until 2015 only states consisting of two or three quarks had been discovered, when an analysis by the LHCb experiment announced the discovery of two pentaquark states, containing five quarks [1]. The observation of pentaquark states is a current field of study in particle physics and especially at the LHCb experiment.

LHCb is one of the four big experiments that are part of the CERN facility in Geneva that houses the largest particle collider in the world, the LHC. The LHCb detector and its functionality are presented in chapter 3.

The first observation of pentaquark states was achieved by the LHCb collaboration in 2015 by providing evidence of the existence of two such states, the $P_c(4380)^+$ and the $P_c(4450)^+$. An update to this finding and evidence of a third pentaquark state, the $P_c(4312)^+$, was published by LHCb this year[2]. The search for pentaquark states and the discoveries so far are discussed in chapter 4. The pentaquarks that have been observed to date, originate from the $J/\Psi p$ channel from $\Lambda_b^0 \rightarrow J/\Psi K^- p$ decays with the quark content of $c\bar{c}uud$. However there are other decays observed at the LHCb that are expected to provide intermediate pentaquark states. For example, the $\Lambda_c^+ \bar{D}^{0(*)}$ channel in $\Lambda_b^0 \rightarrow \Lambda_c^+ \bar{D}^{0(*)} K^-$ decays is a considerable candidate for the observation of pentaquark states with the quark content $c\bar{c}uud$. The high expectation for the P_c to couple to the $\Lambda_c^+ \bar{D}^{0(*)}$ channel results from one of the most popular models for pentaquark states, the model of baryon meson molecules [3]. A feynman diagram of the decay is shown in 1.1.

The focus of this work is the analysis of the decay $\Lambda_b^0 \rightarrow \Lambda_c^+ (\bar{D}^{0*} \rightarrow \bar{D}^0 \pi^0/\gamma) K^-$. Since the π^0 or γ are electrically neutral, they are very difficult to detect at LHCb which leads to the issue that the decay can not be fully reconstructed solely using the information from the detector. The corresponding events can only be partially reconstructed because of the final decay products the π^0/γ are missing which means that crucial information about the decay process gets lost. Therefore these events can not be used to determine whether pentaquark states exist in the $\Lambda_c^+ \bar{D}^{0(*)}$ channel without this information. A previous work provided a method for reconstructing the full decay from the partial information given by

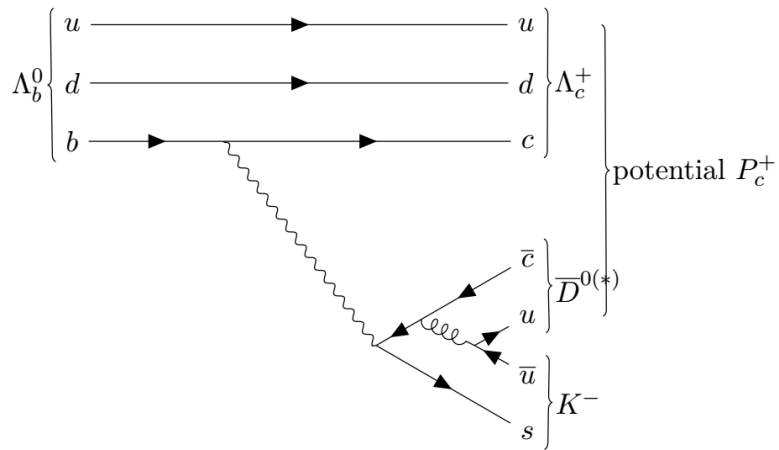


Figure 1.1: Feynman diagram of $\Lambda_b^0 \rightarrow \Lambda_c^+ \bar{D}^{0(*)} K^-$.

the detector. The goal of this bachelor thesis is to provide and test an analysis method for the given decay using the mentioned method for reconstruction of the full decay. Testing and quantifying the efficiency of this method under the assumption of multiple hypotheses by a Monte Carlo study is the first part of this bachelor thesis. Furthermore, a method for dealing with background events in the channel is explored and tested for the decay at hand. In the future, the presented analysis method will be operated on data taken from LHCb.

Introduction to the Standard Model of particle physics

2.1 The particles of the Standard Model

The Standard Model of particle physics summarizes the current knowledge about the structure of matter in a collection of fundamental particles. These fundamental particles can be divided into two categories. There are twelve fermions that matter consists of and five gauge bosons that mediate the interactions between fermions.

2.1.1 The bosons

There are four different kinds of interactions between particles in nature, each associated with different bosons. The gravitational force is not included in the Standard Model, but is insignificant on the scale of particle physics. The electromagnetic interaction between electrically charged fermions is mediated by massless and chargeless photons. The weak interaction between fermions is carried by electrically charged W^+ and W^- bosons and the neutral Z boson. The strong interaction affecting fermions carrying color charge is described by massless and chargeless gluons. The gauge bosons all have spin 1 and are shown in orange in figure 2.1.

2.1.2 The fermions

The twelve fundamental fermions consist of six leptons and six quarks which are grouped into three generations each containing 2 quarks and one charged and one neutral lepton. The electrical charge of the leptons is either 0 or -1 , whereas in each generation there is a quark with charge $-\frac{1}{3}$ and one with $+\frac{2}{3}$. All fermions have spin $\frac{1}{2}$ and an anti-particle with the same mass and spin but opposite charge. They are shown in figure 2.1 sorted into the generations.

The six leptons interact through the weak interaction and if they are electrically charged through the electromagnetic force, while always preserving the electrical charge throughout the interactions. The quarks are affected by all the fundamental forces described in the Standard Model and preserve the baryon number in their interactions which is $+\frac{1}{3}$ for quarks and $-\frac{1}{3}$ for anti-quarks.

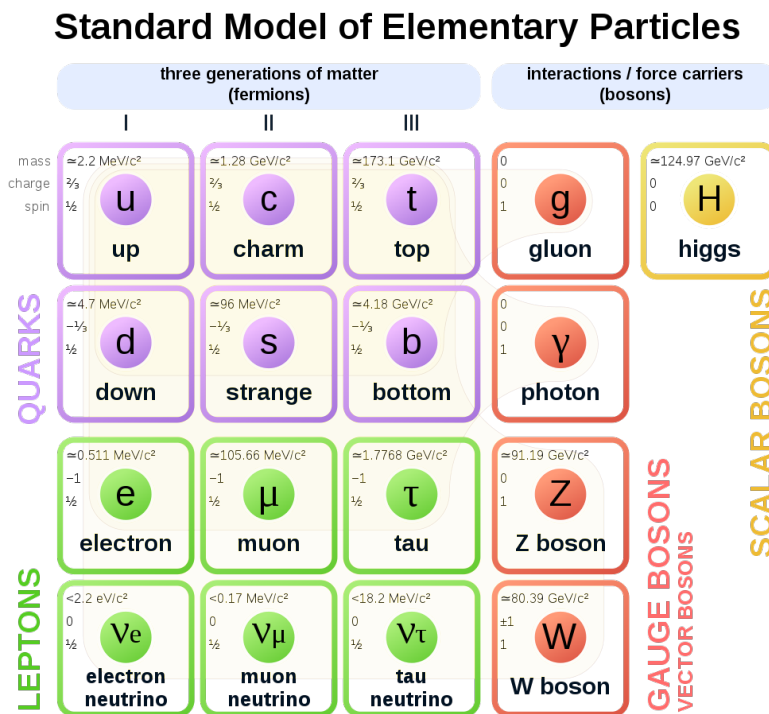


Figure 2.1: The elementary particles in the Standard Model [23].

The most recently discovered element of the Standard Model is the Higgs boson. It has spin 0 which sets it apart from the other bosons in the Standard Model. The Higgs boson mediates the process in which particles gain mass.

2.2 The fundamental forces

The three fundamental forces included in the Standard Model are the electromagnetic force, the weak and the nuclear strong force. There is a theory unifying the electromagnetic and the weak interactions in the electroweak theory and there is an effort to include the strong force as well in which would be a theory describing all interactions in the Standard Model.

2.2.1 The electromagnetic force

The theory describing the electromagnetic force is quantum electrodynamics (QED). It only affects particles with electrical charge which is conserved in all electromagnetic interactions. Since the mediator, the photon, is massless, the electromagnetic force is not spatially restricted which sets it apart from the other fundamental forces. However, the electromagnetic force decreases with distance r by $\frac{1}{r}$.

2.2.2 The weak nuclear force

The weak interaction can affect all fermions in the Standard Model. The theory describing the weak force the best is the electroweak theory which also includes electromagnetic interactions. It is propagated by the W^\pm and Z bosons, which, opposed to photons and gluons, are massive and therefore limit the range of the weak force significantly. Just like the electromagnetic force, the weak force conserves electrical charge in its interactions. Since the weak force is the only fundamental force that can change quark flavor it is essential to many interesting processes. It is also the force responsible for radioactive decays of atoms.

2.2.3 The strong nuclear force

The theory describing the strong force is called quantum chromodynamics (QCD). Only particles with color charge are affected by the strong force which includes quarks and gluons. There are eight gluons carrying color charge and one color neutral gluon which can therefore not mediate the strong force. Three types of color exist that particles can be charged with, red, blue and green, as well as their respective anti-colors. Since only color neutral particle states exist in nature, quarks and gluons are confined in so called hadrons. Attempting to separate quarks from a confined state sets free enough energy for the pair production of a quark and an anti-quark. There are two types of hadrons, baryons and mesons. Baryons consist of three quarks, each carrying a different color charge and therefore being color neutral together. Mesons contain two quarks, a quark and an anti-quark, which also provide a color neutral state by contributing a color and its anti-color.

Detector

3.1 The LHCb Detector

The LHCb detector is designed to study decays from particles containing either bottom or charm quarks (or the respective anti-particles). Since the relevant quarks do not scatter in all directions but stay rather close to the beam line, the detector is not designed around the collision point but rather along the beam line in order to detect the particles of interest and their decay products efficiently. The detector consists of several subdetectors which are aligned behind one another along the beam line. Each of the subdetectors is designed to measure certain properties of the collision particles and their decays. The detector units gather information about the particles' trajectories, their momenta and energies as well as identifying to what particles the tracks belong to and what decay they originated from. The layout of the detector and its subdetectors is displayed in figure 3.1.

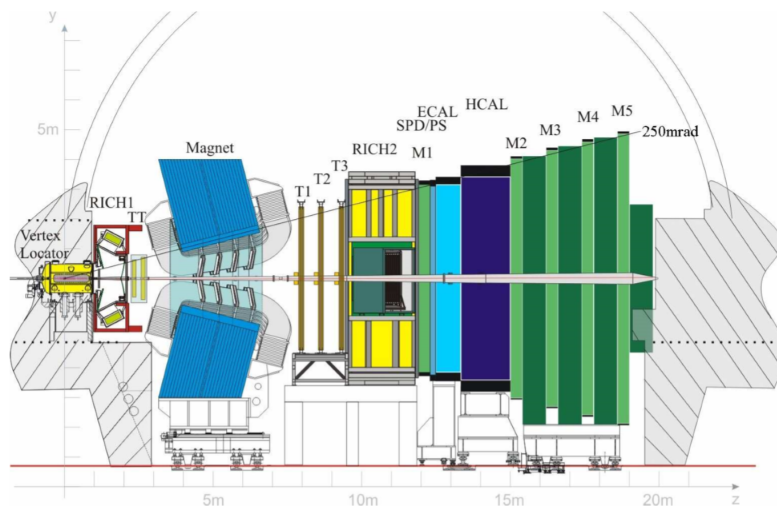


Figure 3.1: Side view of the LHCb detector [20].

The subdetectors are described in the following sections.

3.1.1 VELO

The Vertex Locator (VELO) is the detector unit that is closest to the collision point. The purpose of the Vertex Locator is to measure the trajectory of particles near the proton-proton interactions in order to be able to identify the position of the primary and secondary vertices which are distinctive features of decays of particles with bottom or charm quarks

[4]. It consists of multiple silicon microstrip modules which provide measurements of the r and ϕ coordinates 7 mm from the beam line. Since this is too close to the beam during injection, the VELO halves are movable and can be pulled away from the beam line and are brought back into position once the beam is stable. Each module has one sensor to measure the r coordinate and one sensor to measure the ϕ coordinate.

3.1.2 Silicon Tracker

The Silicon Tracker is made up of two separate detector units, one being located between the collision point and the magnet, the Tracker Turicensis (TT), and one behind the magnet, the Inner Tracker (IT). Both use silicon microstrip detectors, which, in the case of the TT, cover the full acceptance region of the experiment, which is ± 300 mrad horizontally and ± 250 mrad vertically [7]. There are three Inner Tracker units in T1, T2 and T3, however they only cover the area closest to the beam line. The Silicon Trackers are used to calculate the momentum of charged particles from their trajectory before and after passing through the magnetic field of the magnet. Information about the transverse momentum of particles provided from the TT is also used in the High Level Trigger [5].

3.1.3 Magnet

In order to be able to calculate the momentum of charged particles a dipole magnet was installed in LHCb 5.3 meters from the collision area [6]. Charged particles will have a curved trajectory under the influence of a uniform magnetic field. The momentum of the particles can be deduced from the radius of their trajectories while passing the magnetic field. This is why a magnet consisting of two trapezoidal coils was installed which provides an integrated field of 4 Tm and has an acceptance region of 330 mrad horizontally and 250 mrad vertically. The setup of the magnet achieves very accurate momentum measurements for particles with momenta up to 200 GeV/c.

3.1.4 Outer Tracker

The Tracker units T1, T2 and T3 mentioned in the section about the Silicon Trackers consist not only of the Inner Trackers close to the beam line but also of the Outer Trackers which have a different design than the Inner Trackers and cover the area further away from the beam line. The Outer Trackers are designed as multiple straw-tube modules which contain drift-tubes that are used to measure drift time and coordinates. They are used to determine the momentum of charged particles over a larger acceptance area [7].

3.1.5 Calorimeters

The calorimeter system at the LHCb detector includes four separate calorimeters. The Scintillating Pad Detector (SPD), the Pre-Shower Detector (PS), an electromagnetic calorimeter and a hadronic calorimeter. They are used to identify particles as well as to measure their energies and positions. In addition to that, they also provide information about particles for the first trigger level. The electromagnetic calorimeter is used to analyze electrons and photons whereas the hadronic calorimeter is used for hadrons. The separation between photons, electrons and hadrons from other particles is achieved by the SPD and the PS. In the electromagnetic calorimeter there are 66 modules consisting of alternating layers of lead and scintillator tiles [7]. The electrons and photons initiate a shower of particles by interacting with the lead. The shower particles then produce scintillating light in the scintillator tiles which is proportional to the energy of the incoming particle. This is how, for example, the transverse energy of a particle can be calculated in the calorimeter. The hadronic calorimeter is designed similarly except that it uses iron instead of lead tiles for the shower initiation. In each calorimeter the produced light is conveyed by wavelength-shifting fibers and is collected by photomultipliers [8].

3.1.6 Muon Detector

The muon detector system is composed of five stations M1-M5. M1 is located in front of the calorimeter system whereas M2-M5 are placed behind it, each being separated by iron absorbers. M1 is only used in the first trigger level, while the identification and tracing of muons is achieved by stations M2 to M5. A muon signal is only accepted if hits can be found in all five stations that can be assigned to the same particle, in which case the transverse momentum will be calculated by reconstructing the tracks. This is first done in the stations M2 to M5 and if aligning hits are found, the information from M2 and M3 is used to verify whether a corresponding hit was detected in M1 or not. The method yields a resolution of the transverse momentum of approximately 25 %. Since M1 to M3 are utilized to calculate the direction of the track and the transverse momentum, their resolution in the bending plane is higher than in M4 and M5 which mainly serve for the identification of the particles [9].

3.1.7 Ring Imaging Cherenkov Detectors

A crucial part of the analysis done at LHCb is the identification of particles emerging from decays of b -hadrons. In order to be able to separate charged hadronic particles, especially pions and kaons, two Ring Imaging Cherenkov Detectors (RICH) are used. One is placed between the VELO and the magnet while the other sits between the Tracking Systems and the first muon chamber [10]. The identification of charged particles is obviously also

important in the context of the $\Lambda_b^0 \rightarrow \Lambda_c^+ \bar{D}^{0(*)} K^-$ decay. The six final state particles of this decay, which are mostly pions and kaons, have to be correctly identified in order for an event to be registered. Furthermore, since only charged particles can be identified like this, the issue of having uncharged final state particles becomes apparent here. The first RICH detector covers particles with momenta ranging from 1 to 60 GeV/c and takes the full LHCb acceptance. This is achieved by aerogel (only in run 1) and C₄F₁₀ radiators which produce the Cherenkov light. Cherenkov light is emitted from a dielectric medium if a charged particle passes through the medium with a speed that is higher than the speed of light in that medium. This Cherenkov light is then projected through two mirrors to photon detectors which can reconstruct the angle between the particles and the emitted photons. The angle is correlated to the velocity of the incoming particle by:

$$\cos \theta_c = \frac{1}{n \cdot \beta} \quad (3.1)$$

where β is the velocity of the particle divided by c . This yields the velocity of the particles, which, along with information about the momentum gained from the Tracking Systems provide the mass of the particles. The second RICH detector is installed to cover particles with momenta from 15 GeV/c to 100 GeV/c and has a smaller acceptance compared to the first RICH detector, however still covering the region of high momentum particles. The Cherenkov light is emitted from a CF₄ gas radiator and then focused and detected similarly to the first RICH detector. Both RICH detectors are surrounded by magnetic shield boxes since the photon detectors can only operate at full efficiency in magnetic fields much smaller than it would be the case without the shielding due to the LHCb dipole magnet. This is achieved by iron plates that reduce the external field by a factor of around 20. A sketch of the RICH-1 detector is displayed in figure 3.2 [7].

3.1.8 Trigger

LHCb uses two triggers, Level-0 Trigger (L0) and High Level Trigger (HLT), to reduce the events in each bunch crossing significantly and to only store events which are of interest. The L0 is a hardware trigger which operates synchronously to the bunch crossing, while the HLT is a software trigger that only inspects events that passed the L0. The aim of the L0 is to only consider particles with high transversal momentum and energy since mesons with b or \bar{b} quarks often produce these particles. This is achieved by choosing clusters of particles which show the highest transverse energy in the calorimeters or the highest transverse momentum in the muon detectors. This, in addition to information about the number of primary vertices from VELO, defines the L0 and reduces the event rate to 1 MHz at which the whole detector can be read out.

The HLT uses the selections from the L0 and reduces the data even more to 2kHz by utilizing the full read out of the detector in order to determine even better which events

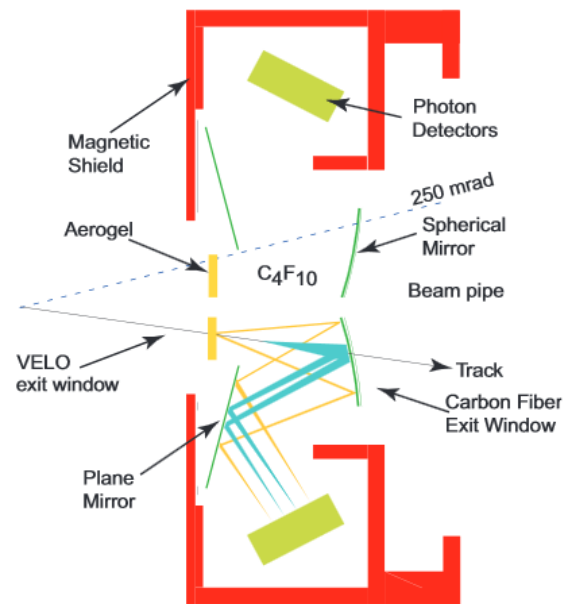


Figure 3.2: A sketch of the first RICH detector [21].

should be stored. It is divided in two levels, the HLT1 and the HLT2. The HLT1 is mainly used to verify events chosen from the L0 trigger by reconstructing the particles in the VELO and the trackers, which reduces the data to about 30 kHz. The HLT2 forms the final stage of the trigger system and eliminates further events that do not fulfill requirements on invariant mass or the direction of the B momentum. This reduces the event rate to about 2 kHz at which the data is stored permanently [7].

Search for exotics

As mentioned in chapter 2, hadrons are split into baryons containing three quarks and mesons consisting of a quark and an anti-quark. However, QCD also allows for other, more complicated states containing more than three quarks. Those states were first proposed by Gell-Mann in 1964 and are called exotic states [11]. Tetraquarks containing two quarks and two anti-quarks and Pentaquarks containing four quarks and one anti-quark are such states and are subject to modern particle physics research. States with more than five quarks have been proposed and looked for as well, however there have been no observations of such states to date. The first observation of an exotic state was the $Z(4430)^\pm$ which was discovered in 2008 by the Belle Collaboration in B decays and has a minimal quark content of $c\bar{c}d\bar{u}$. It was found in the $\pi^\pm\Psi'$ channel in the decay $B \rightarrow K \pi^\pm \Psi'$ [12]. In 2015, this observation was confirmed by LHCb with the measurements of the mass and the width of the $Z(4430)^-$ being improved [13].

4.1 Pentaquark search

The first claim of having observed a pentaquark occurred in 2002, when the Laser-Electron-Photon collaboration announced they had found evidence of the existence of a pentaquark they named Ψ^+ . The Ψ^+ was claimed to have a mass of $1.54 \text{ GeV}/c^2$ and a quark content of $uudd\bar{s}$, however other experiments could not confirm the existence of the Ψ^+ when they would have been expected to [14]. The first observation of a pentaquark state was achieved by LHCb in 2015. They published observations of the $J/\Psi p$ channel from $\Lambda_b^0 \rightarrow J/\Psi K^- p$ decays where they measured two resonances corresponding to pentaquark states. The observed pentaquarks include a charm and an anti-charm quark which is why they are called charmonium pentaquarks and are labeled P_c^+ . The quark content of the P_c^+ is $c\bar{c}uud$. The two resonances, that were measured with a significance of more than nine standard deviations, occurred at masses of $4380 \text{ MeV}/c^2$ and $4449.8 \text{ MeV}/c^2$ [1]. The most recent discovery of a pentaquark state also came from LHCb in 2019. In an analysis of the same channel from the same decays compared to the observations in 2015, however in a larger data sample, a new pentaquark state with a mass of 4311.9 MeV was observed with a significance of 7.3 standard deviations. Furthermore, the $P_c(4450)^+$ state observed in 2015 was discovered to be an overlay of two P_c^+ states with a significance of 5.4 standard deviations and masses of 4440.3 MeV and 4457.3 MeV . [2]

4.2 Pentaquark models

Since the observations of pentaquark states by LHCb, a vividly discussed and researched topic is how such states are bound and how they can be described. One of the proposed models are strongly bound systems. There are multiple concepts for strongly bound systems such as a diquark-triquark combination in which a pentaquark would consist of a state of two quarks and a state of three that are bound together by gluons. Another, similar concept is an actual pentaquark system. Furthermore, a molecular concept is heavily present in modern research. This model considers pentaquarks to behave like molecules of a baryon and a meson.

The $\Lambda_b^0 \rightarrow \Lambda_c^+ \bar{D}^{0(*)} K^-$ decay

5.1 The $\Lambda_b^0 \rightarrow \Lambda_c^+ \bar{D}^0 K^-$ analysis

So far, all experimental observations of the P_c^+ state by LHCb originate from the $J/\Psi p$ channel in Λ_b^0 decays. However, it can be expected for the P_c^+ to couple to other two- and three-body channels that offer the corresponding quark content. Amongst those expected channels are the $P_c^+ \rightarrow \bar{D}^{0*} \Lambda_c^+$ and $P_c^+ \rightarrow \bar{D}^0 \Lambda_c^+$ [19]. As mentioned before, there are multiple models for describing the nature of pentaquark states. The most popular interpretations to date are strongly bound systems, like diquark triquark systems, and baryon meson molecules. The latter predicts large cross sections for the decay of the P_c^+ to $\bar{D}^{0*} \Lambda_c^+$ and $\bar{D}^0 \Lambda_c^+$ [3]. These predictions lead to an analysis by LHCb of the $\Lambda_b^0 \rightarrow \Lambda_c^+ \bar{D}^0 K^-$ decay using run 1 data in 2018. The resulting mass distribution of signal events is displayed in figure 5.1.

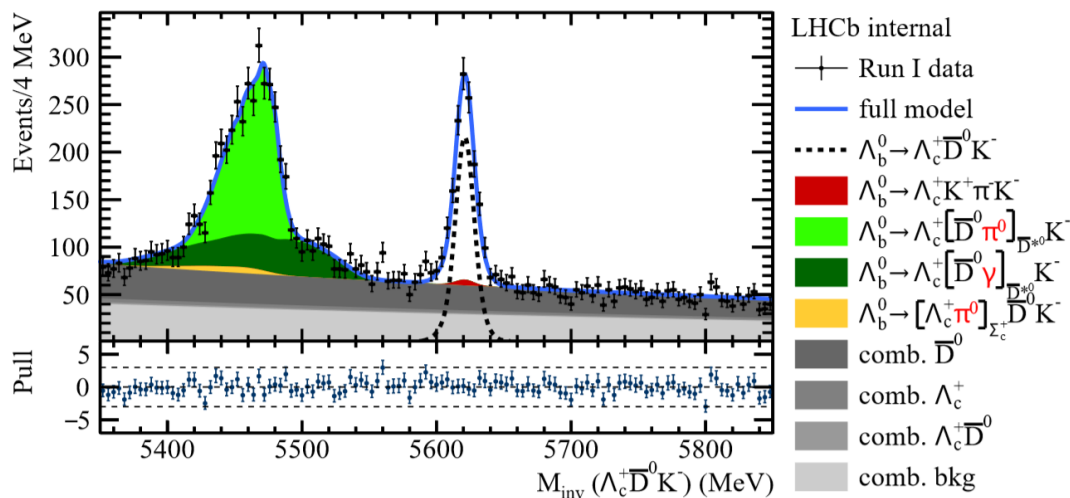


Figure 5.1: Mass distribution of reconstructed Λ_b^0 [22].

The mass of the Λ_b^0 is listed as 5619.6 MeV by the PDG [18], which is also where a resonance occurs in figure 5.1. However, a significant portion of events yield an invariant mass which is approximately 160 MeV smaller than the mass of the mother particle of

the decay, the Λ_b^0 . This means that somewhere in the detection and analysis process this amount of energy must have been lost.

5.2 $\bar{D}^{0*} \rightarrow \bar{D}^0 \pi^0/\gamma$

An explanation for the events that yield a lower mass is that the decay was actually $\Lambda_b^0 \rightarrow \Lambda_c^+ \bar{D}^{0*} K^-$ and that the \bar{D}^{0*} decayed into $\bar{D}^0 \pi^0$ or $\bar{D}^0 \gamma$. The π^0 and the γ are electrically neutral and therefore difficult to detect, which means that there is either no or little information about those particles available. This implies that only the \bar{D}^0 , Λ_c^+ and K^- are being recorded by the detector which is the same information one would obtain from $\Lambda_b^0 \rightarrow \Lambda_c^+ \bar{D}^0 K^-$ decays. The reconstruction of the mass of the Λ_b^0 in $\Lambda_b^0 \rightarrow \Lambda_c^+ \bar{D}^{0*} K^-$ decays will be lacking the energy of the missing particle which leads to the observed shift towards lower masses for the reconstructed Λ_b^0 in figure 5.1. Since only a part of the decay products is used to reconstruct the Λ_b^0 mass, the concerned events are referred to as partially reconstructed. The full decay channel for those cases would be $\Lambda_b^0 \rightarrow \Lambda_c^+ (\bar{D}^{0*} \rightarrow \bar{D}^0 \pi^0/\gamma) K^-$. The fact that either a γ or a π^0 get lost in the detection leads to issues in the analysis of this full decay channel which will be addressed in the following chapters.

Analysis Strategy

The ultimate goal of the analysis is to determine whether pentaquark states exist in the $\Lambda_c^+ \bar{D}^{0(*)}$ channel in $\Lambda_b^0 \rightarrow \Lambda_c^0 \bar{D}^{0(*)} K^-$ decays. By using the partially reconstructed events from the $\Lambda_b^0 \rightarrow \Lambda_c^+ \bar{D}^0 K^-$ analysis it can be expanded. This can be achieved by using a reconstruction method that can obtain the \bar{D}^{0*} from the decay products that are detected and analyzed. This has certain implications on the analysis process of the $\Lambda_c^+ \bar{D}^{0(*)}$ channel which are to be determined and quantified in this bachelor thesis.

6.1 Reconstruction of the \bar{D}^{0*}

The difficulty of analyzing the $\Lambda_b^0 \rightarrow \Lambda_c^+ (\bar{D}^{0*} \rightarrow \bar{D}^0 \pi^0/\gamma) K^-$ channel is the loss of information about some of the final decay products, namely the π^0 and the γ . This is due to the fact that both the π^0 and the γ are electrically neutral and are therefore not as easily and precisely detected by the LHCb detector. A possible solution to this problem is reconstructing the lost information from the decay particles that are actually detected. This is done by using a variation of a closed cone method designed for the reconstruction of missing neutrinos. The performance of this reconstruction method is crucial to the analysis of this decay and is tested and analyzed in this bachelor thesis. One particular feature of the reconstruction method is the fixing of the mass of the missing particle. This means, that when using the method to reconstruct the missing energy of the decay, one has to make either the assumption that the missing particle was a π^0 or that it was a γ . Since it is impossible to determine whether a π^0 or a γ is missing for one specific event, there are four cases that can arise when applying the method to a given event. One can apply the reconstruction under the assumption that a π^0 is lost, which can either be the case or a γ was actually lost that was now treated as a π . Similarly, when using the reconstruction under the hypothesis of a missing γ , it could either be the correct hypothesis or a π is now being reconstructed as if it were a γ . This results in four different cases that all have to be taken into consideration when utilizing the reconstruction method in the analysis of this decay. The occurring cases are displayed in table 6.1.

Occured decay	Reconstructed decay	
$\bar{D}^{0*} \rightarrow \bar{D}^0 \pi^0$	π^0	γ
$\bar{D}^{0*} \rightarrow \bar{D}^0 \gamma$	γ	π^0

Table 6.1: Possible choices of the reconstruction particle.

This will lead to the analysis being divided into two parts for each event. A given event will have to be analysed under the hypothesis that a γ was lost as well as the hypothesis that a π was lost. One important aspect of the analysis is the efficiency of the reconstruction method for each of the cases presented in table 6.1. This is further discussed and examined in chapter 7.

6.2 Dalitz plot

A very helpful tool for determining whether such an intermediate state exists in a three-body-decay is a so called Dalitz plot. A Dalitz plot is a visual representation of the phase-space of a three-body-decay. Since the kinematics of such a decay can be described by two variables, a Dalitz plot is two dimensional. Suppose a particle decays into the decay products A, B, C. Then, the two axes of the plot are the squares of the invariant masses of two pairs of the decay products, which could for example be m_{AB}^2 and m_{BC}^2 . Each decay is then plotted in this two-dimensional plot depending on the invariant masses of the decay products that are measured. The choice of the axes depends on the channel one wants to examine. In the $\Lambda_b^0 \rightarrow \Lambda_c^+ \bar{D}^{0(*)} K^-$ decay the events would for example be plotted as functions of $m_{\Lambda_c^+ \bar{D}^{0(*)}}^2$ and $m_{D^{0(*)} K^-}^2$ since the pentaquark state is expected to couple to the $\Lambda_c^+ \bar{D}^{0(*)}$ channel. In general, if all involved particles had spin 0 and there were no intermediate states, the events in the Dalitz plot are homogeneously distributed within the kinematically allowed region. The edge of this region is called the boundary of the Dalitz plot. Such a Dalitz plot is provided in figure 6.1a. If there is a intermediate state in a three-body-decay, the density of the Dalitz plot will peak at the mass of the intermediate state in the corresponding channel. A good example for this is the decay of $\Lambda_b^0 \rightarrow \Lambda_c^+ (D_s^*(2700)^- \rightarrow \bar{D}^{0*} K^-)$. The distribution in the $D^{0*} K^-$ channel in the Dalitz plot will show a resonance at the mass of the $D_s^*(2700)^-$ which, according to the PDG [18], is 2708.3 MeV. This resonance will be visible as a band in the Dalitz plot, which is displayed in figure 6.1.

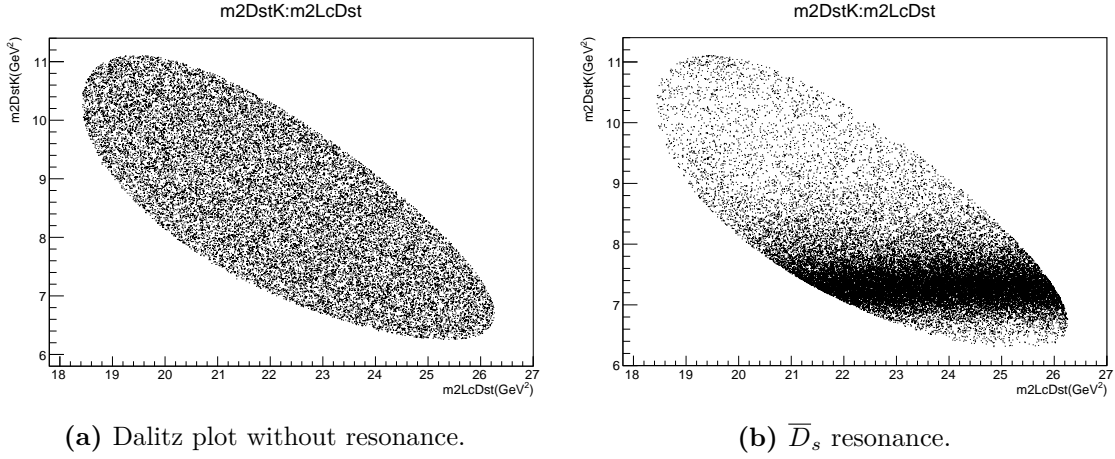


Figure 6.1: Examples for Dalitz plots.

6.3 Monte Carlo Data

A very convenient tool for testing an analysis before applying it on real data is Monte Carlo (MC) data. Monte Carlo data for a certain decay consists of simulated events which means that the decay one wants to study is simulated for a certain number of times by a program which will provide a dataset of the decay that can be obtained without relying on real events. This is obviously limited by how well the process of a certain decay is understood. Not only are the kinematics of the decays simulated, but also the process of the detection of the decay products. This includes efficiencies and finite detector resolution. This way analysis methods can be tested on MC data representing real data without being limited by the availability thereof. One big advantage of MC studies is that the dataset which a certain method is tested on can be much larger than a real dataset.

6.4 Generation of a dataset for $\Lambda_b^0 \rightarrow \Lambda_c^+ \bar{D}^{0*} K^-$

The events on which the analysis tools in this work are tested on originate from Monte Carlo data which was generated with the simulation RapidSim [24]. RapidSim is designed for phase space decays of hadrons containing bottom and charm quarks and can simulate the process of a decay in the LHCb detector [15]. In the following the MC data was created for $\Lambda_b^0 \rightarrow \Lambda_c^+ (\bar{D}_s^{*}(2700)^- \rightarrow (\bar{D}^{0*} \rightarrow \bar{D}^0 \pi^0/\gamma) K^-)$ which includes the detector simulation. Since this represents the events that can only be partially reconstructed, the reconstruction method has to be applied to the given data in order to get a Dalitz plot like above. In figures 6.2a and 6.2b $\Lambda_b^0 \rightarrow \Lambda_c^+ (\bar{D}^{0*} \rightarrow \bar{D}^0 \pi^0) K^-$ was simulated while in figures 6.2c and 6.2d $\Lambda_b^0 \rightarrow \Lambda_c^+ (\bar{D}^{0*} \rightarrow \bar{D}^0 \gamma) K^-$ was simulated. Since the γ and π^0 would not be registered in real events the reconstruction method needs to be applied on these two datasets, which can each be done under both hypotheses. This results in four

cases, similar to table 6.1, and four Dalitz plots which are displayed in figure 6.2. In figure 6.2a the missing π was reconstructed as a π whereas in 6.2b the reconstruction assumed a missing γ . Similarly, in 6.2c the missing γ was assumed to be a γ and in 6.2d it was treated as a missing π .

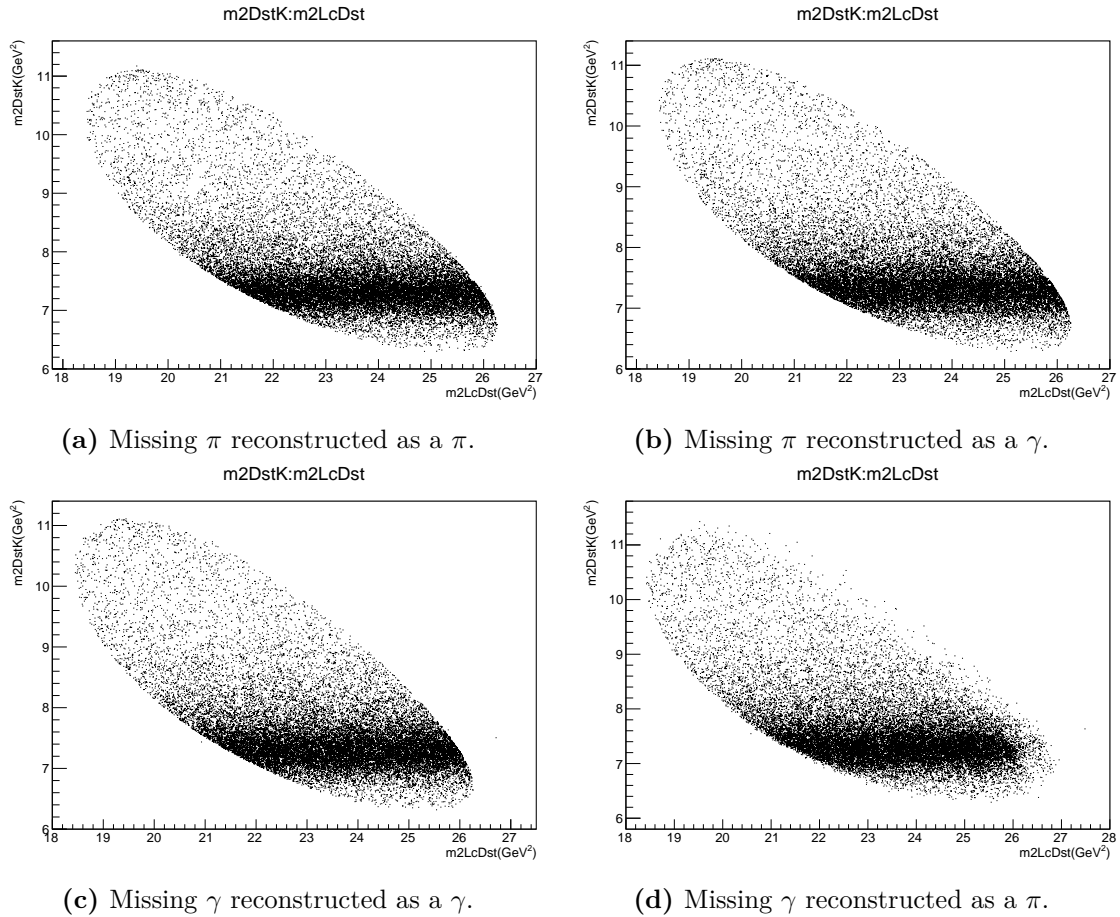


Figure 6.2: Dalitz plots after reconstruction.

In all cases the resonance from the D_s in the $D^{0*} K^-$ channel is still visible. However, it is noticeable that the reconstruction has a significant impact on the distribution of the events. Especially in figure 6.2d, it is obvious that at least the reconstruction under the wrong hypothesis is clearly affecting the edges of the Dalitz plot with some events placing outside of the boundaries of the Dalitz plot. This is further examined in chapter 7. In chapter 8 a closer analysis is described which focuses on how the reconstruction affects the distribution in the Dalitz plot. This is described as the resolution of the Dalitz plot which is crucial in the analysis of this decay channel.

In the real analysis it is obviously not possible to distinguish between events that include a missing π and events with a missing γ . Therefore, the dataset that is to be analysed will contain both kinds of decays. According to the PDG the $D^*(2007)^0$ has the two decay modes $D^0 \pi^0$ and $D^0 \gamma$ with decay fractions of 64.7% and 35.3% [18]. A realistic dataset

would therefore consist of 64.7% events with a missing π and 35.3% events with a missing γ . In figure 6.3 a MC dataset simulating exactly that is displayed in the same Dalitz plot as above. In figure 6.3a the reconstruction used assumed a missing π and in figure 6.3b the γ hypothesis was made. Therefore, in both Dalitz plots the correct reconstruction was used on some of the data while on others the wrong one was applied.

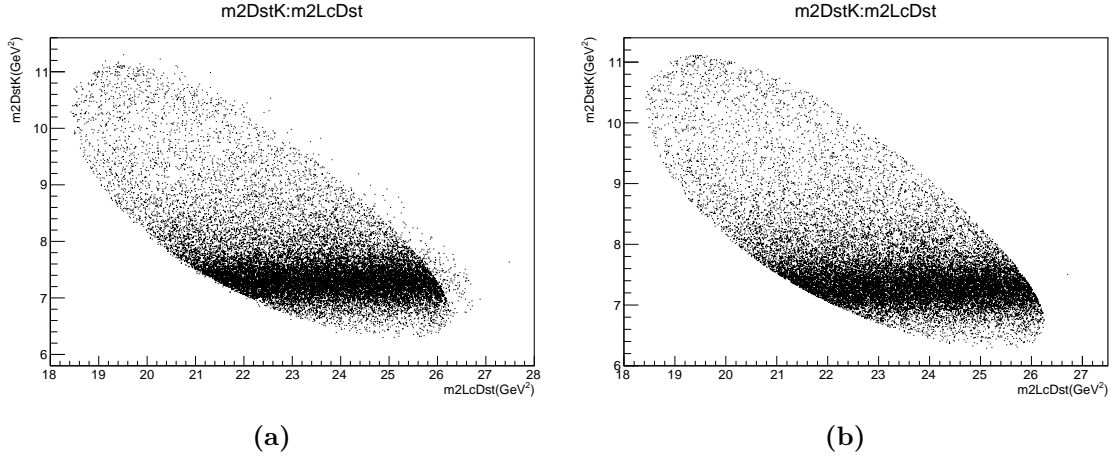


Figure 6.3: Dalitz plots of mixed events reconstructed as a π^0 (a) and a γ (b).

In addition to the events originating from the decay $\Lambda_b^0 \rightarrow \Lambda_c^+ \bar{D}^{0(*)} K^-$ also background events will have to be considered. In figure 5.1 this is represented by the grey areas. For this examination background was created from simulation as well. The background was generated as combinatorial background from the simulation of the $\Lambda_b^0 \rightarrow \Lambda_c^+ \bar{D}^{0(*)} K^-$ decay. This is achieved by combining information about single particles from different signal events to generate a background event. This obviously has very little to do with the actual background, however general studies about the background can still be performed on this basis. In figure 6.4 the dataset from figure 6.3 was extended with 15% of background events. Again, figure 6.4a displays the reconstruction with the π hypothesis while 6.4b assumes a missing γ .

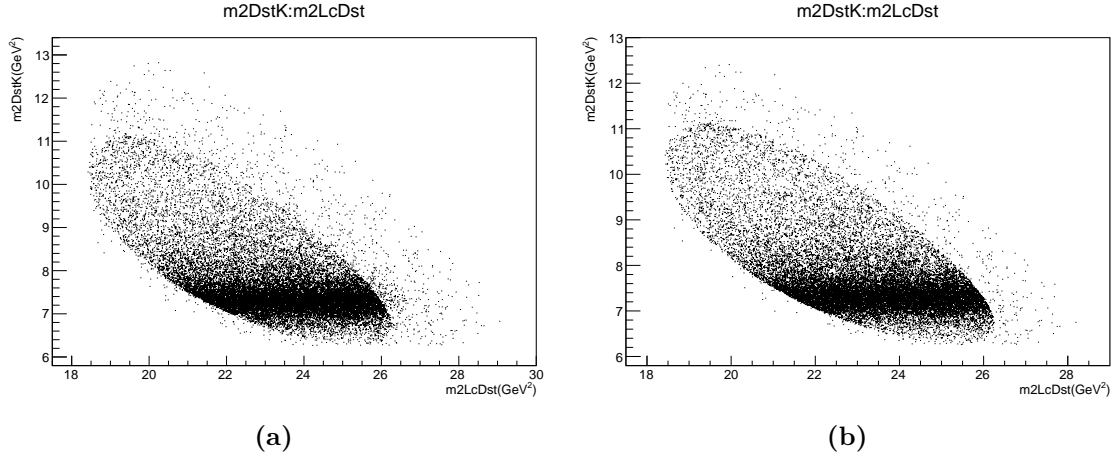


Figure 6.4: Dalitz plots of mixed events with background reconstructed as a π^0 (a) and a γ (b).

A method for dealing with and eliminating the background is examined and discussed in chapter 9. This forms the final part of what is necessary to analyze this decay channel. With the information gathered in the steps above, it is now possible to create probability density functions (PDF) describing the Dalitz plots for decays of this kind.

6.5 Probability density function

The goal of the analysis is to create and model PDFs by analyzing reconstructed Dalitz plots in the variables $m_{\Lambda_c^+ \bar{D}^{0*}}^2$ and $m_{\bar{D}^{0*} K^-}^2$. These PDFs would then be used to determine whether a pentaquark resonance can be observed in the $\Lambda_b^0 \rightarrow \Lambda_c^+ (\bar{D}^{0*} \rightarrow \bar{D}^0 \pi^0/\gamma) K^-$ channel. This would be visible through an interference of the three possible sub-decays:

$$\Lambda_b^0 \rightarrow \bar{D}^{0*} (\Xi_c^0 \rightarrow \Lambda_c^+ K^-)$$

$$\Lambda_b^0 \rightarrow \Lambda_c^+ (\bar{D}_s^{0*} \rightarrow \bar{D}^{0*} K^-)$$

$$\Lambda_b^0 \rightarrow K^- (P_c \rightarrow \bar{D}^{0*} \Lambda_c^+)$$

Since it is not possible to distinguish whether a π^0 or a γ needs to be reconstructed, one will get two Dalitz plots, one for the reconstruction with a π^0 and one for the reconstruction with a γ . As laid out above, both Dalitz plots will be made up of multiple contributions. Each of the Dalitz plots contain events that included a π^0 which was not detected and events that included a γ which was not detected as well as background events. Since a different hypothesis is used in the two Dalitz plots, the contributions to the PDFs describing the distribution in the Dalitz plots will be different as well. Each PDF will therefore consist

of three unique terms. This includes one correctly applied hypothesis, one wrongly applied hypothesis and one background term. The two functions will have the following form:

$$PDF_{\pi} = N_{\pi} \cdot \int R_{\pi}^{\pi} \cdot A_{\pi}^2 + N_{\gamma} \cdot \int R_{\pi}^{\gamma} \cdot A_{\gamma}^2 + N_{bkg} \cdot PDF(bkg)_1 \quad (6.1)$$

$$PDF_{\gamma} = N_{\gamma} \cdot \int R_{\gamma}^{\gamma} \cdot A_{\gamma}^2 + N_{\pi} \cdot \int R_{\gamma}^{\pi} \cdot A_{\pi}^2 + N_{bkg} \cdot PDF(bkg)_2 \quad (6.2)$$

In both cases $A_{\pi/\gamma} = |A_{D_s} + A_{\chi_c} + A_{P_c}|$ with $A_{...}$ the signal models of the three possible sub-decays depending on which particles the \bar{D}^{0*} decayed into (π or γ).

N_{π} , N_{γ} and N_{bkg} are the respective fraction yields of the π signal, γ signal and the background. R_{π}^{γ} , R_{π}^{π} , R_{γ}^{γ} and R_{γ}^{π} are the resolutions of the corresponding Dalitz plots. The lower indices express which reconstruction was used whereas the upper indices mark which particle resulted from the $\bar{D}^{0*} \rightarrow \bar{D}^0 \pi^0/\gamma$ decay. The resolution takes into account how the position of an event in the Dalitz plot is changed through the reconstruction of the missing particle. The resolution is then folded with the above described signal models since a position in the Dalitz plot is also influenced by the signal model in the area around it because of the resolution. Depending on the resolution not the whole area of the Dalitz plot has to be taken into account since the influence of areas that have a certain distance to an event can be neglected. If this is the case, only the area closest to an event has to be used for this which is achieved by the integral of the product of $R \cdot A^2$ over the desired area. This is examined closer in section 8.3.

Efficiency of the reconstruction method

The first aspect one can consider for the events that are reconstructed is the mass of the Λ_b^0 that the reconstruction yields. The reconstructed mass can be utilized to classify events before the analysis is performed. The conditions that the reconstructed mass has to fulfill and their effects are described in this chapter.

The reconstructed Λ_b^0 mass is obtained from the masses and momenta of the Λ_c^+ , the K^- and the reconstructed \bar{D}^{0*} . If the reconstruction is accurate and was used correctly, the mass should always yield 5619.60 ± 0.17 MeV, which is the mass of the Λ_b^0 as given by the PDG[18]. By eliminating events that do not yield a reconstructed Λ_b^0 mass lying within three standard deviations of the PDG value, unreasonable events can be dropped. This is one aspect of the efficiency of the reconstruction method because it eradicates events that are reconstructed inaccurately. With the cut on the Λ_b^0 mass applied, the reconstruction was run on five different MC sets, each containing 100000 signal events of one of the signal species. The results for the efficiency is listed in table 7.1 in the column “Efficiency” with statistical errors.

A second aspect that can be taken into account is, that when the π^0 hypothesis is applied, the Λ_b^0 mass of the partially reconstructed channel has to be smaller than the mass of the Λ_b by the rest mass of the π^0 which is 134.98 MeV according to the PDG [18]. Therefore, when applying the π^0 hypothesis all those events can be ignored, that yield a partially reconstructed mass that is higher than 5484.62 MeV. There is no lower limit on the partially reconstructed mass because the π^0 can be created with a momentum. This additional cut was applied to the MC data for the π^0 hypothesis and the fractions of events that made the cut are listed as “ π cut” in table 7.1 with statistical errors.

Missing particle	Hypothesis	π cut	Efficiency
γ	γ	-	0.97 ± 0.01
γ	π	0.65 ± 0.02	0.59 ± 0.02
π	π	0.97 ± 0.02	0.99 ± 0.01
π	γ	-	0.99 ± 0.01

Table 7.1: Efficiency of reconstruction method.

In the case of a missing γ reconstructed as a π , the restrictions seem to eliminate 61% events that are wrongly reconstructed. In those cases only the Dalitz plot using the γ hypothesis will have to be considered. For the cases where the correct reconstruction

was used, the efficiency of the reconstruction method is around 97% which means, that under the correct hypothesis most signal events will be kept. Although three percent of correctly reconstructed events are eliminated through the cuts, the statistics for the search for pentaquarks in the $\Lambda_c^+ \bar{D}^{*0}$ channel are still sufficient.

An additional benefit of these two restrictions is, that they help eliminate some of the background in both Dalitz plots. After applying them to the full MC dataset including the π^0 and γ signal types and background events the Dalitz plots from figure 6.4 now have the following form:

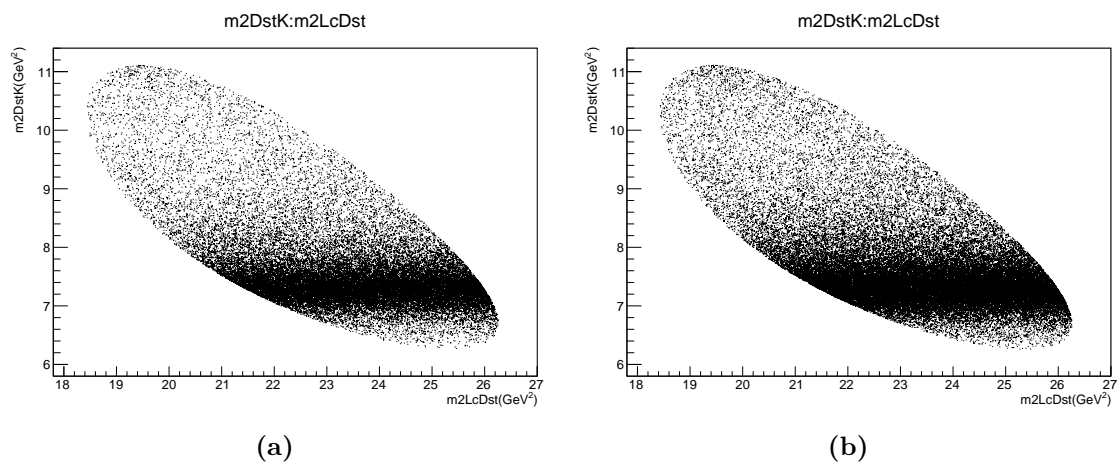


Figure 7.1: Dalitz plots of mixed events with background reconstructed as a π^0 (a) and a γ (b).

In both cases, events that previously were outside of the boundaries of the Dalitz plot do not meet the requirements mentioned above and are therefore not considered. The analysis can be exclusively performed within the boundaries of the Dalitz plot, because based on the reconstruction, events that lay outside of the kinematically allowed region are rejected.

Resolution

The two axes of the Dalitz plot, $m_{\Lambda_c \bar{D}^{0(*)}}^2$ and $m_{\bar{D}^{0(*)} K^-}^2$, both involve the mass of the \bar{D}^{0*} . Since the mass of the \bar{D}^{0*} is calculated through a reconstruction method, the accuracy of the position of an event in the Dalitz plot depends on the performance of the reconstruction. Examining and quantifying this influence is the subject of this chapter.

The manner in which the position is affected by the reconstruction is henceforth called the resolution of the reconstruction in the Dalitz plot. The resolution has a large significance when creating a PDF that describes the distribution of events in the Dalitz plot as presented in section 6.5. As laid out in chapter 7 the relevant events will be located inside the boundaries of the Dalitz plot which means that the resolution needs to be determined only for that area as well.

While in a real dataset only information about the \bar{D}^0 is available, when performed on MC data the true values for the four vector of the \bar{D}^{0*} can be calculated and used for testing. The true values from the MC simulation can then be compared to the ones that the reconstruction yields. For each event the values of the Dalitz plot variables can on the one hand be calculated with the reconstructed \bar{D}^{0*} , which will yield the values $m_{\Lambda_c \bar{D}^{0*}}^2$ and $m_{\bar{D}^{0*} K^-}^2$. On the other hand they can be calculated with the true values from the MC simulation, which will yield $m_{\Lambda_c \bar{D}^{0*}, \text{true}}^2$ and $m_{\bar{D}^{0*} K^-, \text{true}}^2$. By comparing these values, the effect of the reconstruction on the Dalitz plot variables can be quantified. Calculating the difference between the values for each event is the first step towards calculating the resolution.

$$\Delta m_{\Lambda_c \bar{D}^{0*}}^2 = m_{\Lambda_c \bar{D}^{0*}, \text{true}}^2 - m_{\Lambda_c \bar{D}^{0*}}^2 \quad (8.1)$$

$$\Delta m_{K^- \bar{D}^{0*}}^2 = m_{K^- \bar{D}^{0*}, \text{true}}^2 - m_{K^- \bar{D}^{0*}}^2 \quad (8.2)$$

In order to get the resolution, the area of the Dalitz plot is divided into two-dimensional bins. The goal is to determine the distribution of the differences $\Delta m_{\Lambda_c \bar{D}^{0*}}^2$ and $\Delta m_{K^- \bar{D}^{0*}}^2$ for all bins in the Dalitz plot. Therefore the differences are calculated for each event and collected in the corresponding bins based on the true values of the variables. This is done on the whole dataset, after which the data is depicted as two histograms for each available bin, one for $\Delta m_{\Lambda_c \bar{D}^{0*}}^2$ and one for $\Delta m_{K^- \bar{D}^{0*}}^2$. An example of two such histograms for one bin containing the described data is given in figure 8.1.

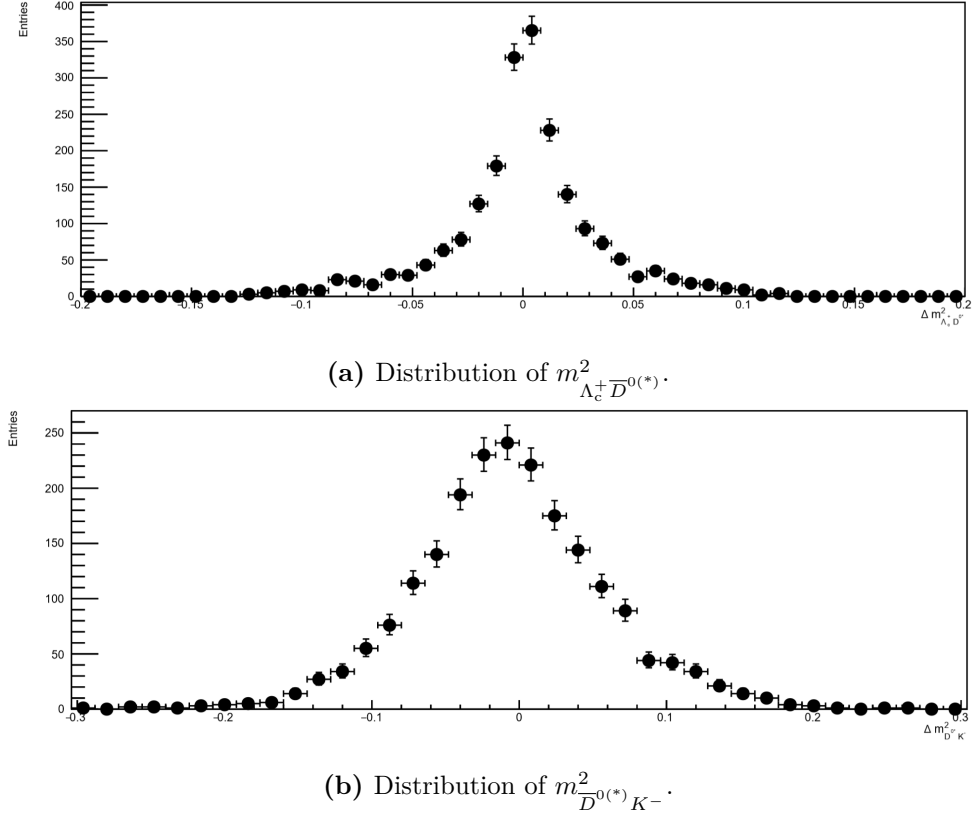


Figure 8.1: The differences $m^2_{\Lambda_c^+ \bar{D}^{0(*)}}$ (a) and $m^2_{\bar{D}^{0(*)} K^-}$ (b) for one generic bin in the Dalitz plot displayed as histograms.

8.1 Resolution Model

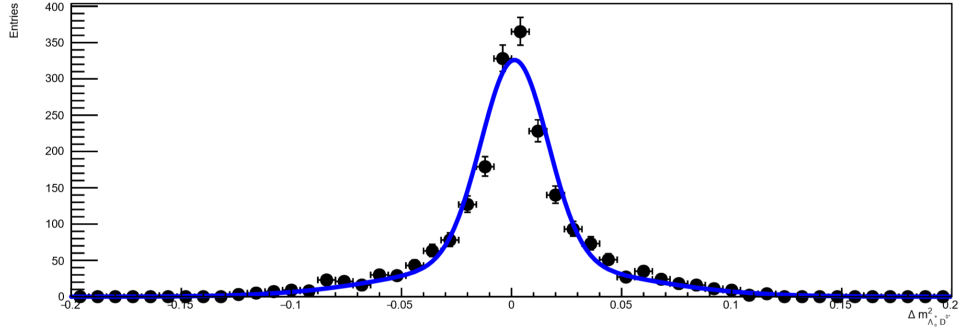
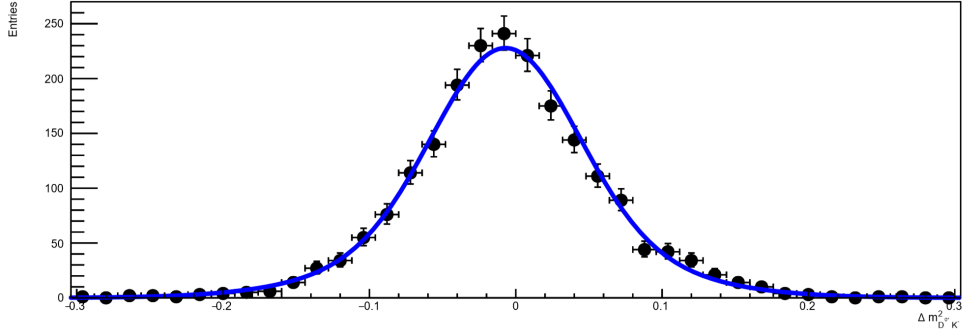
In order for this information to be used in equations 6.1 and 6.2, the distribution of the differences in all bins have to be modeled with a function. In the case of figure 8.1 both histograms can be described by a double gaussian which is defined by the sum of two gaussians that share the same mean μ but have separate widths σ_1 and σ_2 . It has the form:

$$DG(x) = a_1 \cdot G(x; \mu, \sigma_1) + a_2 \cdot G(x; \mu, \sigma_2) \quad (8.3)$$

with

$$G(x; \mu, \sigma) = \frac{1}{\sqrt{2 \cdot \pi} \cdot \sigma} \cdot e^{-\frac{(x-\mu)^2}{2 \cdot \sigma^2}} \quad (8.4)$$

The model is applied to both histograms with unique values for a_1, σ_1, μ, a_2 and σ_2 and added to the data in figure 8.2.

(a) Model for the resolution of $m_{\Lambda_c^+ \bar{D}^{0(*)}}^2$.(b) Model for the resolution of $m_{\bar{D}^{0(*)} K^-}^2$.**Figure 8.2:** Model for the resolution in a generic bin of the Dalitz plot.

Since the double-gaussian models seem to describe the data in both variables well, the two-dimensional resolution of a bin can be written as a product of two double gaussians.

$$R(x, y) = (a_1 \cdot G(x; \mu_1, \sigma_1) + a_2 G(x; \mu_1, \sigma_2)) \cdot (a_3 \cdot G(y; \mu_2, \sigma_3) + a_4 \cdot G(y; \mu_2, \sigma_4)) \quad (8.5)$$

with x and y being the two Dalitz plot variables. This yields a two-dimensional model for a bin in the Dalitz plot that can describe the resolution of events in that bin. This has to be done separately for every bin in the Dalitz plot by fitting the function 8.5 to the data in each of them.

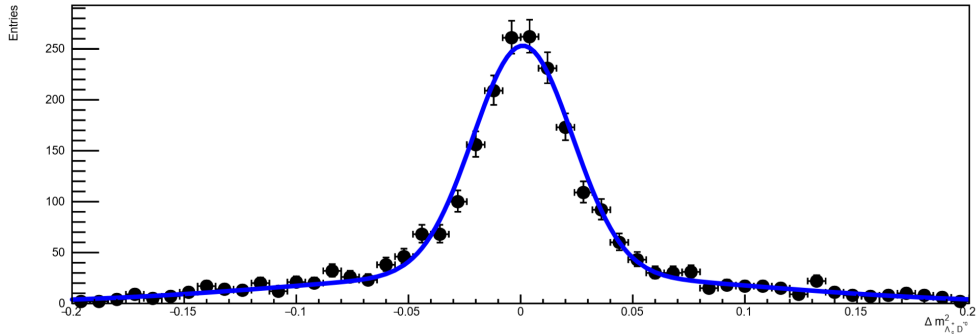
8.2 Different cases

The above depicted data was generated from a MC sample that simulated $\bar{D}^{0*} \rightarrow \bar{D}^0 \gamma$ and was reconstructed under the hypothesis of a missing γ . Since the choice of the hypothesis and the occurred decay play a significant role for the resolution of the Dalitz plot, the other cases as mentioned in table 6.1 have to be examined as well. All four possible combinations will have a unique resolution and are important when trying to describe the distribution of

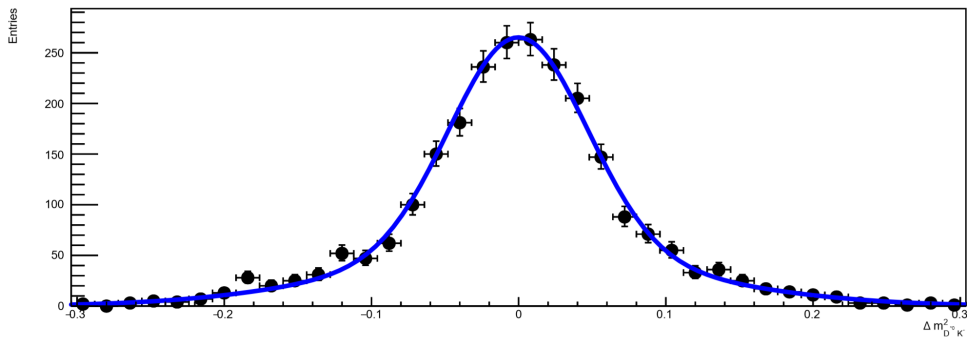
events in the Dalitz plot. In the PDFs for the Dalitz plots in formulas 6.1 and 6.2 they were labeled as R_{π}^{γ} , R_{π}^{π} , R_{γ}^{γ} and R_{γ}^{π} , where the lower index marks the applied hypothesis whereas the upper index indicates the particle that was created. The procedure described in chapter 8 so far has to be conducted for all these cases. The question that arises, is, whether the proposed model in section 8.1 can appropriately describe all four occurring combinations of missing particles and hypotheses.

To determine this, all bins that the Dalitz plot is divided into have to be examined. Judging from figure 7.1, the relevant area of the Dalitz plot ranges from 6 to 11.5 GeV^2 in $m_{D^{0(*)}K^{-}}^2$ and from 18 to 27 GeV^2 in $m_{\Lambda_c^+D^{0(*)}}^2$. The y -axis is divided into twelve bins with the width 0.5 GeV^2 while the x -axis is divided into ten bins with a width of 1 GeV^2 . Not all bins in this rectangular division of the Dalitz plot will be relevant since some of them cover areas that lie out of the boundaries of the Dalitz plot. For those bins and the ones that lie on the edge of the kinematically allowed area, and therefore have too little data to make a statistically relevant statement, the resolution does not have to be determined.

In the case of the correct hypothesis being used, so for R_{π}^{π} , as can be seen in figure 8.3, and R_{γ}^{γ} , as can be seen in figure 8.2, $\Delta m_{\Lambda_c^+D^{0(*)}}^2$ and $\Delta m_{K^-D^{0(*)}}^2$ seem to be distributed according to formula 8.5 in all available bins. By determining the parameters $a_1, \sigma_1, \mu_1, a_2, \sigma_2, a_3, \sigma_3, \mu_2, a_4, \sigma_4$ for these cases the resolutions R_{π}^{π} and R_{γ}^{γ} can be defined for all bins in the Dalitz plot and applied to the PDF of the Dalitz plot.



(a) Model for the resolution of $m_{\Lambda_c^+D^{0(*)}}^2$



(b) Model for the resolution of $m_{D^{0(*)}K^-}^2$

Figure 8.3: Model for the resolution R_{π}^{π} in a generic bin of the Dalitz plot

For the cases in which the wrong hypothesis was used, R_π^γ and R_π^π , this does not seem to be true anymore for all bins, as can be seen in figure 8.4. Although there are a few bins where the model 8.5 can be described with simple models, similar to 8.5, the data in most of the bins show very few similarities and the distributions of $\Delta m_{\Lambda_c^+ \bar{D}^{0*}}^2$ and $\Delta m_{K^- \bar{D}^{0*}}^2$ have no obvious correlations.

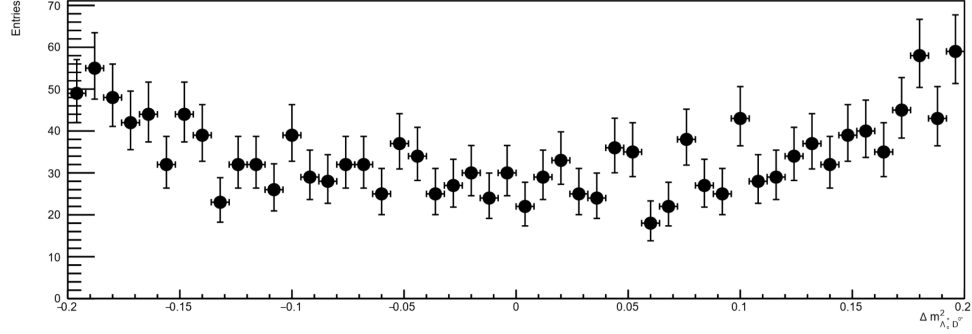
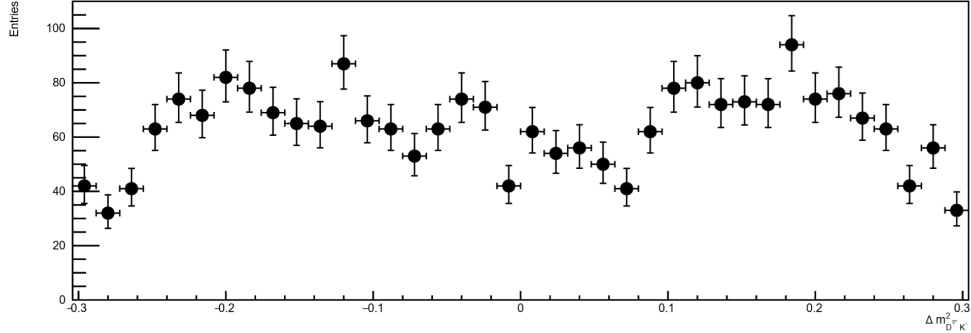
(a) Resolution of $m_{\Lambda_c^+ \bar{D}^{0(*)}}^2$ (b) Resolution of $m_{D^{0(*)} K^-}^2$

Figure 8.4: The differences $m_{\Lambda_c^+ \bar{D}^{0(*)}}^2$ (a) and $m_{D^{0(*)} K^-}^2$ (b) for one generic bin in the Dalitz plot displayed as histograms for R_π^γ

For these bins individual models have to be determined that can describe the given data appropriately.

8.3 Range

Because of the limited resolution, the position of an event in the Dalitz plot is inaccurate to some degree. Events that have been assigned a certain position would have had a different position if the reconstruction had not been needed. This is why, when calculating the value of the PDF for a position, the surrounding area has a significant effect. This is represented by the integral of the product of the resolution and the amplitude model over the relevant area. The size of the area that needs to be considered depends on the resolution, which is why only bins within a certain range of a position have to be included. Bins with a

greater distance do not have a significant effect. The necessary range of the integral can be determined from the values resulting from the model fits as described in section 8.2. The maximal distance $\Delta m_{\Lambda_c^+ \bar{D}^{0*}}^2$ or $\Delta m_{K^- \bar{D}^{0*}}^2$ that occurs, even for R_π^γ and R_γ^π , is 0.2 GeV². This means that for a given position in the Dalitz plot, it will be sufficient to take the resolution models of only the closest bins surrounding that position into account, considering the size of the bins.

Background

One crucial aspect of the analysis of this channel is the subtraction of the background. As one can see in figure 5.1, there is a significant amount of background in the decay channel, mainly being combinatorial background. A common technique for the reduction of background is the sWeight technique. Whether this method can be applied to the given dataset in order to reduce the background and enhance the signal quality is the focus of this chapter.

9.1 sPlot technique

The sPlot technique is designed to deal with datasets with multiple contributions that one wants to separate as is the case for the given decay. It is used to determine the distribution of variables whose distribution is unknown for all of the event contributions. This is done by choosing sets of variables from the data which are then divided into two components. The first component consists of variables for which the distribution of the events for all sources is known. These are called discriminating variables. The second component, the control variables, consists of variables for which the distribution is not known for at least one of the contributions. The distributions for the control variables are then determined by assigning weights to the events based on the distribution in the discriminating variables. These weights, the so called sWeights, are calculated for every event source and from those the distribution in the control variables can be calculated. Since sWeights are calculated for all contributions, their values can be negative or positive depending on how likely an event originates from a contribution.

In the case of the $\Lambda_b^0 \rightarrow \Lambda_c^+ (\bar{D}^{0*} \rightarrow \bar{D}^0 \pi^0/\gamma) K^-$ decay, the sources of events would be the events that yield a π , the events that yield a γ and background events which are characterized in figure 5.1. The discriminating variable in this case would be the partially reconstructed mass of the Λ_b^0 for which the distribution is known for the involved contributions. An essential assumption when using the sPlot technique is that the control variables are uncorrelated to the discriminating variable [16]. However, this is not the case in the presented analysis. In the reconstruction method that is applied, the mass of the Λ_b^0 is used to compute the \bar{D}^{0*} . Since the control variables are $m_{\Lambda_c^+ \bar{D}^{0*}}^2$ and $m_{\bar{D}^{0*} K^-}^2$ and the \bar{D}^{0*} is part of them, the control variables in this case are correlated to the discriminating variable through the reconstruction of the \bar{D}^{0*} .

This raises the question whether the sPlot technique can be applied to this decay or not since one of the assumptions on which it is based is not fulfilled.

9.2 From sWeights to probabilities

The method of checking whether the sPlot technique can be applied in this case is based on a machine learning method. When using machine learning methods with sWeighted data the fact that sWeights are designed to be negative as well as positive becomes an issue. This concerns loss functions on which machine learning methods are based. When using negative sWeights, loss functions can become unbounded and therefore the training of machine learning methods will not converge. This is why the weights obtained from an sPlot need to be transformed into classical probabilities for them to be used in such a method. There are different approaches for this depending on the statistics available and the number of control variables.

9.3 sWeight averaging

One way of transforming the sWeights to probabilities is by calculating the average over events with the same values for the control variables. If x are the control variables, the probability of getting a signal event for certain values of x , which are also called features, is $w(x) = \frac{p_{\text{signal}}(x)}{p_{\text{mix}}(x)}$. When using sWeights that were calculated from a discriminating variable m , the signal probability for an event with certain features x would be the average over events with those features, $\mathbf{E}(\text{sWeight}(x, m)) = w(x)$ [17]. This can obviously only be achieved if there is enough statistics for all features x for the average to be calculated. Since the Dalitz plot area is divided into bins and there will only be a few thousand events in the real dataset, this method can not be applied on the real data, because there will not be enough data to determine the averages correctly. However, with MC data this is possible, which offers a method of checking whether sWeighting can be used in this context or not.

This test was done on a MC dataset containing 100000 events of which 20% were simulated background as described in section 6.4 and 80% were $\Lambda_b^0 \rightarrow \Lambda_c^+ (\bar{D}^{0*} \rightarrow \bar{D}^0 \gamma) K^-$ events. The events were labeled accordingly before being merged into a single dataset. Firstly, a model was created for describing the distribution of the dataset in the discriminating variable, the partially reconstructed mass of Λ_b^0 , which consists of a model of $\Lambda_b^0 \rightarrow \Lambda_c^+ (\bar{D}^{0*} \rightarrow \bar{D}^0 \gamma) K^-$ and a polynomial background contribution. This model was then fitted to the distribution of the events in the partially reconstructed Λ_b^0 mass which is displayed in figure 9.1.

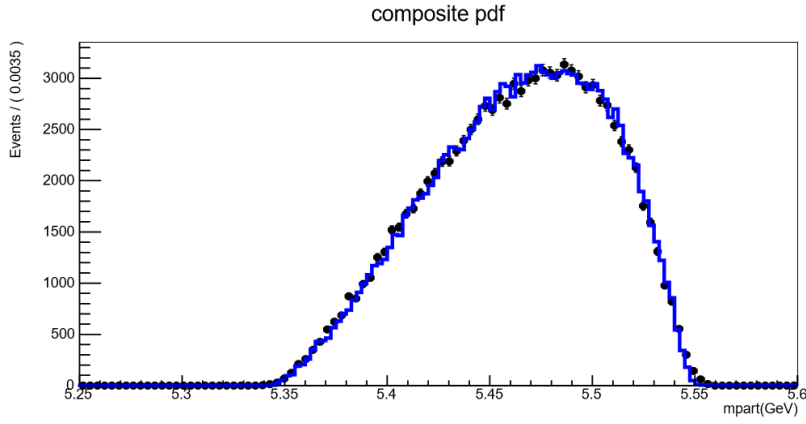


Figure 9.1: Data (black) and model (blue) of partially reconstructed Λ_b^0 mass distribution.

From this distribution the sWeights for the events were calculated. The Dalitz plot was then, once again, divided into bins. Events that are placed in the same bin are treated as if they had the same features. This way the average of the sWeights can be calculated for each bin. On the other hand, each event was labeled before being mixed which offers the opportunity of calculating the classical probability for signal and background events for each bin. If the sPlot technique is valid for this dataset, although the control variables are correlated to the discriminating variable, the probabilities generated from the two methods should be the same. In figure 9.2 the classically calculated probabilities are displayed for the signal (a) and the background (b).

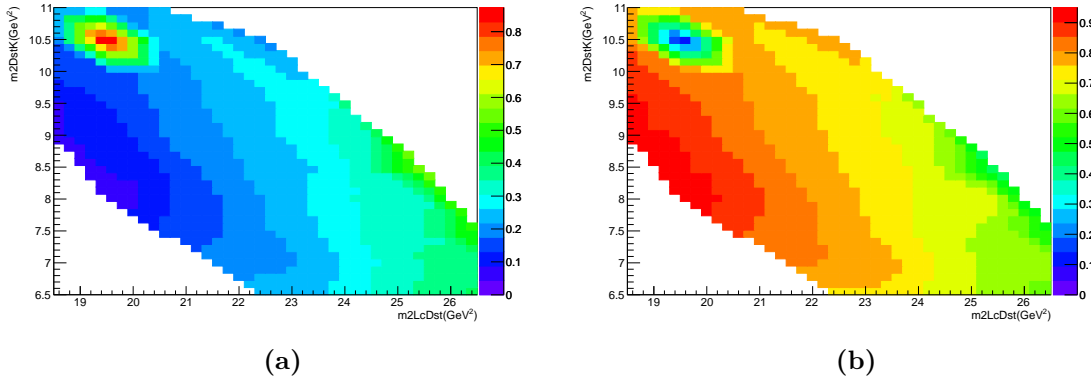


Figure 9.2: Classical probabilities for the bins in the Dalitz plot for signal (a) and background (b).

In figure 9.3 the averages of the sWeights for each bin are displayed.

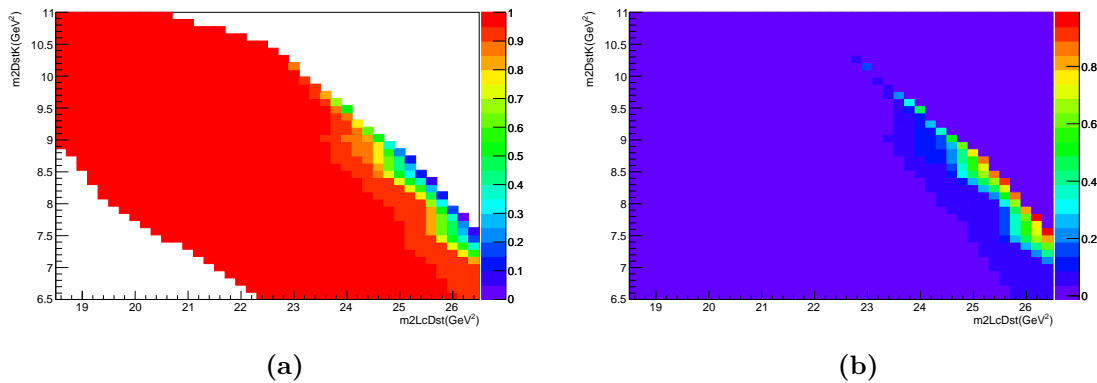


Figure 9.3: For each bin in the Dalitz plot the average of the signal sWeights (a) and the background sWeights (b) were calculated.

By comparing the two plots for the signal weights it becomes obvious, that the averaged sWeights do not manage to reproduce the classical probabilities for signal and background distribution. The whole relevant area of the Dalitz plot basically yields an sWeight average of 1 which coincides only with the classically calculated probabilities on the lower edge. Especially for high values of the x -axis and low values of the y -axis the classical probability and the averaged sWeights do not match.

This means that the proposed method is inadequate for handling the background in this channel. There are however other methods which can be examined. For example, the background in the sideband of the partially reconstructed Λ_b^0 mass distribution (see figure 5.1) could be extrapolated and used to describe the background in the relevant area.

Conclusion and Outlook

In the search for pentaquark states, LHCb conducted an analysis of the $\Lambda_b^0 \rightarrow \Lambda_c^+ \bar{D}^0 K^-$ decay because a pentaquark state was predicted in the channel $P_c^+ \rightarrow \bar{D}^{0(*)} \Lambda_c^+$. It was found, that a considerable amount of data yielded a reconstructed Λ_b^0 mass that was between 100 and 200 MeV smaller than the expected value. This is due to the fact that the Λ_b^0 mass of the decay $\Lambda_b^0 \rightarrow \Lambda_c^+ (\bar{D}^{0*} \rightarrow \bar{D}^0 \pi^0/\gamma) K^-$ is only partially reconstructed. In order to properly reconstruct these events, a variation of a closed cone method is applied to the detected final particles. A premise for this method is, that the mass of the missing particle has to be given. Since it is not possible to distinguish between the missing γ and the missing π^0 , the events have to be reconstructed under both hypotheses.

A resonance in the Dalitz plot with the coordinates $m_{\Lambda_c \bar{D}^{0(*)}}^2$ and $m_{\bar{D}^{0(*)} K^-}^2$ could indicate an intermediate pentaquark state [6.2]. Because of this, probability density functions describing the distribution of the events in the Dalitz plot are needed. Since the data has to be reconstructed under two hypotheses, two PDFs are needed to describe the reconstructed data [6.5].

The resolution of the Dalitz plot is an important part of the PDFs and was the focus of this work [8]. It describes the effect of the reconstruction on the events' position in the Dalitz plot. Four different resolutions had to be calculated since there are two possible missing particles and two hypotheses that can be applied. The resolutions R_π^π and R_γ^γ were determined by calculating the distributions of the differences $\Delta m_{\Lambda_c \bar{D}^{0*}}^2$ and $\Delta m_{K^- \bar{D}^{0*}}^2$ in bins of the Dalitz plot and could be modeled with the product of two double Gaussians. For the resolutions R_γ^π and R_π^γ the distributions were calculated as well, however there was no obvious model they could be fitted with [8.2].

In order to minimize the number of events that are wrongly reconstructed, two cuts on the reconstruction were introduced, concerning the partially and fully reconstructed Λ_b^0 mass. By applying the cuts, a large number (fraction) of events that are reconstructed under the wrong hypothesis can be eliminated, 61.65%. The correctly reconstructed events are barely affected, of them only 3% are eliminated.[7.1]

Lastly, the sPlot technique was tested on the presented decay [9]. Since the Dalitz plot variables are not independent of the partially reconstructed Λ_b^0 mass, one of the premises of the sPlot technique was disregarded. This was tested by comparing the averages of the sWeights to classical probabilities in the Dalitz plot. If the sPlot technique was applicable to the decay, the averaged sWeights should have agreed with the probabilities. This could then have been used to estimate the background distribution in the Dalitz plot. However, the sWeights failed to reproduce the probabilities, which is why a different method will have to be used for the background subtraction. If such a method and a model for R_γ^π and R_π^γ can be found, the presented analysis strategy could be applied to the given data.

Bibliography

- [1] LHCb Collaboration, R. Aaij et al., "Observation of $J/\psi p$ Resonances Consistent with Pentaquark States in $\Lambda_b^0 \rightarrow J/\psi K^- p$ Decays", Phys. Rev. Lett. 115, 072001, arXiv:1507.03414 [hep-ex].
- [2] LHCb Collaboration, R. Aaij et al., "Observation of a narrow pentaquark state, $P_c(4312)^+$, and two-peak structure of the $P_c(4450)^+$ ", arXiv:1904.03947v2 [hep-ex].
- [3] M. Gell-Mann, "A Schematic Model of Baryons and Mesons", Phys. Lett. 8 (1964) 214-215.
- [4] R.Dzhelyadin, On behalf of the LHCb Collaboration, "The LHCb calorimeter detectors", PACS: 29.40 Vj; 29.40.Mc.
- [5] C.W. Shen, Y.H. Lin, "Decay behaviors of the P_c hadronic molecules", arXiv:1710.09037 [hep-ph].
- [6] J. André et al., "Status of the LHCb Magnet System", IEEE Transactions on Applied Superconductivity Volume 12 Issue 1.
- [7] M. Borisyak, N. Kazeev, "Machine Learning on data with sPlot background subtraction", arXiv:1905.11719v4 [cs.LG].
- [8] A A Alves Jr et al., "Performance of the LHCb muon system", JINST 8 P02022.
- [9] Kenneth H. Hicks, "On the conundrum of the pentaquark", Eur. Phys. J. H 37, 1-31 (2012).
- [10] M. Adinolfi et al., "Performance of the LHCb RICH detector at the LHC", Eur. Phys. J. C(2013) 73:2431.
- [11] Particle Data Group Collaboration, M. Tanabashi et al., "Review of Particle Physics", Phys. Rev. D98 no. 3, (2018) 030001.
- [12] G.A. Cowan et al., "RapidSim: an application for the fast simulation of heavy-quark hadron decays", arXiv:1612.07489v2 [hep-ex].
- [13] Olaf Steinkamp, On behalf of the LHCb Collaboration, "Silicon strip detectors for the LHCb experiment", PACS: 29.40.Gz;29.40.Wk.
- [14] M. Pivk and F.R. Le Diberder, "sPlot: a statistical tool to unfold data distributions", arXiv:physics/0402083v3 [physics.data-an].
- [15] LHCb Collaboration, R. Aaij et al., "Observation of the Resonant Character of the $Z(4430)^-$ State", Phys. Rev. Lett. 112.222002.

-
- [16] Belle Collaboration, S.-K Choi et al., "Observation of a Resonancelike Structure in the $\pi^{+-}\psi'$ Mass Distribution in Exclusive $B \rightarrow K\pi^{+-}\psi'$ Decays", Phys. Rev. Lett. 100, 142001.
- [17] LHCb Collaboration et al., "The LHCb Detector at the LHC", JINST 3 S08005.
- [18] R. Aaij et al., "Performance of the LHCb Vertex Locator", JINST 9 P09007.
- [19] T.J. Burns, "Phenomenology of $P_c(4380)^+$, $P_c(4450)^+$ and related states", Eur. Phys. J. A (2015)51: 152.
- [20] "Webpage: LHCb detector along the bending plane.", <https://commons.wikimedia.org/wiki/File:Lhcbview.jpg>. Accessed: 2019-07-10.
- [21] "Webpage: RICH detectors", <http://lhcb-public.web.cern.ch/lhcb-public/en/Detector/RICH2-en.html>. Accessed: 2019-07-16.
- [22] M. Stahl, First observation of the decay $\Lambda_b^0 \rightarrow \Lambda_c^+ \bar{D}^{(*)0} K^-$ in preparation of a pentaquark search in the $\Lambda_c^+ \bar{D}^{(*)0}$ system at the LHCb experiment, PhD thesis, Heidelberg U.
- [23] "Webpage: Standard model of elementary particles.", <https://commons.wikimedia.org/wiki/File:Standard-Model-of-Elementary-Particles.svg>. Accessed: 2019-07-10.
- [24] "Webpage: gcowan/RapidSim", <https://github.com/gcowan/RapidSim>. Accessed: 2019-07-05.

Acknowledgements

Firstly, I want to thank Sebastian Neubert for letting me write my bachelor thesis in his group and under his supervision and for the guidance and patience he showed me. Secondly, I would like to thank Nicola Skidmore for proof-reading my work and helping me to present it in an appropriate way. I also want to thank my two office partners, Fabian Glaser and Pallav Mohan, for offering a helping hand when necessary and sharing laughs during the breaks. A huge credit also goes to the Studienstiftung des deutschen Volkes for creating opportunities to meet other students and supporting me financially. Lastly, I want to thank Mathieu Kaltschmidt, Carl von Randow and Alexander Müller for proof-reading and making the last three years incredibly enjoyable and my parents for making this amazing opportunity possible in the first place.

Declaration of Authorship

I hereby certify that this thesis has been composed by me and is based on my own work, unless stated otherwise.

Heidelberg, _____